Stochastic Downscaling of Hourly Precipitation Series From Climate Change Projections

Ziwen Yu[1] [ID], **Franco Montalto[2], Stefan Jacobson[3], Upmanu Lall[4]** [ID], **Daniel Bader[4]** [ID], and **Radley Horton[4]**

[1]University of Florida, Gainesville, FL, USA, [2]Drexel University, Philadelphia, PA, USA, [3]Philadelphia Water Department, Philadelphia, PA, USA, [4]Columbia University, New York, NY, USA

Abstract Stochastic precipitation generators (SPGs) are often used to produce synthetic precipitation series for water resource management. Typically, an SPG assumes a stationary climate. We present an hourly precipitation generation algorithm for nonstationary conditions informed by the global climate model (GCM) forecasted average monthly temperature (AMT). The physical basis for precipitation formation is considered explicitly in the design of the algorithm using hourly pressure change events (PCE) to define the relationship between hourly precipitation and AMT. The algorithm consists of a multivariable Markov Chain and a moving window driven by time, temperature, and pressure change. We demonstrate the methodology by generating a 100-year, continuous, synthetic hourly precipitation time series using GCM AMT projections for the Northeast United States. When compared with historical observations, the synthetic results suggest that future precipitation in this region will be more variable, with more frequent mild events and fewer but intensified extremes, especially in warm seasons. The synthetic time series suggests that there will be less precipitation in the summers, while winters will be wetter, consistent with other research on climate change projections for the Northeast United States. This SPG provides physically plausible weather ensembles for water resource studies involving climate change.

1. Introduction

The anthropogenic use of fossil fuels releases greenhouse gases (GHGs) into the atmosphere, contributing to global warming (Solomon et al., 2007; US EPA Environmental Protection Agency, 2010; VijayaVenkataRaman et al., 2012). Global climate models (GCMs) suggest that increased GHG emissions could alter precipitation patterns, with associated impacts on the reliability and performance of water resource infrastructure. These impacts could be particularly acute in urban settings, where even small changes in the intensity and duration of precipitation can result in pronounced changes in runoff due to the proliferation of impervious surfaces (Betts et al., 2007; Hamlet & Lettenmaier, 1999; Huntington, 2003; Labat et al., 2004). Changes in precipitation patterns can also alter urban flood risks (Pfister et al., 2004; Schreider et al., 2000), change the volume and frequency of combined sewer overflows (CSOs) (Nie et al., 2009; Semadeni-Davies et al., 2008), and impact the performance of the billion dollars green infrastructure (GI) programs implemented in an increasing number of North American cities (Gill et al., 2007).

Global warming is very likely to increase precipitation potential due both to acceleration of evaporation and an increase in the air holding capacity of the atmosphere (K. E. Trenberth, 2011; Solomon et al., 2007). In theory, a one-degree Celsius change in air temperature can bring about a 7% increase in the air's moisture-holding capacity. The Clausius-Clapeyron (CC) relationship extends this increase in the air holding capacity to the global scale under climate change (Sun et al., 2007; Trenberth & Shea, 2005). The actual relationship between temperature and air holding capacity has been investigated using measured climatic data at monthly (King et al., 2014; Trenberth & Shea, 2005), daily (Sun et al., 2007; Westra, Alexander, & Zwiers, 2013), and subdaily (G. Lenderink & van Meijgaard, 2010; Lenderink & van Meijgaard, 2008) timescales. Researchers have also investigated how changes in air temperature alter mean (Allen & Ingram, 2002; K. E. Trenberth, 2011) and extreme (Groisman et al., 2005; Kunkel et al., 2013; Meehl et al., 2005; Meehl et al., 2012; Shaw et al., 2011) precipitation amounts, as well as event durations (Panthou et al., 2014; Wasko, Sharma, & Johnson, 2015).

At relatively coarse temporal (e.g., decadal, annual, or seasonal) and spatial (e.g., continental or regional) scales, GCMs can be used to investigate how different emission scenarios might alter precipitation patterns. Precipitation is, however, the GCM output with the greatest bias relative to observations (Johnson & Sharma, 2009;

Kendon et al., 2008). The use of GCM outputs in predicting precipitation at finer temporal (e.g., daily, hourly, and subhourly) and spatial scales (e.g., local and mesoscale) is generally considered inappropriate, in large part due to the inability of GCMs to accurately simulate precipitation intensity and resolve localized weather patterns (Mamalakis et al., 2017; Teutschbein & Seibert, 2013).

At finer temporal and spatial scales, GCM outputs can be dynamically downscaled into regional climate models (RCMs) and/or incorporated into stochastic precipitation generators (SPG) (Fowler et al., 2007; Wilks, 2010) in different ways. SPGs have been used to incorporate precipitation uncertainty and variability into the evaluation of flood risks (Haberlandt et al., 2008), the reliability of rainwater harvesting systems (Basinger et al., 2010), and the effectiveness of other water resource decisions (Shamir et al., 2015). In stationary applications, a variety of techniques can be employed to generate multiple Markovian sequences of precipitation, for example, ensembles (Wilks & Wilby, 1999). Parametric methods utilize statistical distributions of wet-day rain volumes (Stern & Coe, 1984; Wilks, 1998), precipitation arrival time, intensity, duration (Rodriguez-Iturbe et al., 1987, 1988; Wasko & Sharma, 2017; Wasko, Pui, et al., 2015), and other rain event characteristics (Heneker et al., 2001). Nonparametric methods, by contrast, create synthetic sequences by strategically sampling historical precipitation (Basinger et al., 2010; Lall & Sharma, 1996; Lall et al., 1996; Sharma & Lall, 1999), for example, within a moving window to preserve seasonality (Rajagopalan et al., 1996).

In many applications, especially those requiring fine temporal precipitation quantities (e.g., urban stormwater planning), the direct use of GCM-forecasted precipitation in SPGs is not appropriate since GCMs poorly reproduce precipitation event intensity (Johnson & Sharma, 2009, 2012), especially during extreme events (Kim et al., 2020). However, GCM forecasts of future annual, seasonal, or monthly precipitation amounts are routinely compared to historical precipitation to generate delta change factors (at annual, monthly, or seasonal scales) that can be used to modify historical event characteristics. Maimone et al. (2019), for example, developed an SPG to stochastically generate future sequences of hourly precipitation for 2080–2100 by inflating historical rainfall amounts by factors derived from an analysis of multiple GCM predictions of annual and seasonal precipitation for Philadelphia.

Whether they are parametric or nonparametric, and regardless of whether they are being used to create ensembles of historical or future precipitation, SPG sampling procedures typically make a static assumption regarding the physical processes causing the formation of precipitation. Such assumptions can be defended under a stationary climate, but as the atmosphere warms drivers of precipitation could change. Although the accuracy of precipitation forecasts under climate change could be improved by considering the fundamental physical mechanisms of precipitation formation, dynamic simulation of convection processes remains challenging (Westra, Evans, et al., 2013).

Precipitation is caused when moist air rises, cools, condenses, and coalesces into droplets that can fall under the right conditions (Evans & Westra, 2012; Westra, Evans, et al., 2013). The dynamic relationships between precipitation, temperature, and pressure were generalized by Ahrens et al. (2012) who showed that air pressure at the ground surface is consistently reduced as air is lifted. At small (e.g., local and/or mesoscale) spatial scales, Hoxit et al. (1976) found that surface pressure dropped due to the formation of convective clouds. Ahrens et al. (2012) and Visser et al. (2020) presented temperature changes associated with the onset of an extreme precipitation event in the Australian tropics. These processes vary even at subdaily timescales (Evans & Westra, 2012) with "no a priori reason" to assume consistency in a future climate (Westra, Evans, et al., 2013). In Yu et al. (2018), we suggest the use of pressure changes as potential predictors of future nonstationary precipitation formation.

In this paper, we present a nonparametric SPG for nonstationary future precipitation. The SPG generates dynamic sequences of hourly precipitation using GCM predictions of future Average Monthly Temperature (AMT). The algorithm is based on the meteorological relationships between precipitation and temperature involving pressure changes, as originally introduced by Yu et al. (2018). One of the purposes of this study is to demonstrate that using pressure changes, SPG algorithms can be used to preserve the physical causality of precipitation in a nonstationary generator.

The paper is structured as follows. First, we describe the data sources used and the relationship between hourly precipitation and AMT. Next, the stochastic precipitation generation algorithm is introduced, followed by a validation of the model outputs using pooled gauge data across the Northeast United States as a test case.

2. Data Sources and Collection

The study focuses on the Northeastern coastal United States: A coastal region extending from Philadelphia to Boston characterized by mostly flat terrain (See Figure A1 in Appendix A). Throughout this region, the vertical lifting of air is typically associated with frontal precipitation rather than orographic lifting. Over 50 years of high-quality, hourly measurements of temperature, precipitation, and sea level air pressure were obtained from the National Climate Data Center (NCDC) (formerly the National Center for Environmental Information) at stations located at the international airports in New York City (NYC) (station ID: 72503014732 for 1973–2018 and 99999914732 for 1948–1973), Philadelphia (PHL) (station ID: 72408013739 for 1973–2018 and 99999913739 for 1941–1973), and Boston (BOS) (station ID: 72509014739 for 1943–2018) (See Figure A1 in Appendix A). Since topographic relief and climatic conditions vary little across the region, data from all three cities were pooled into one data set. This pooling also increased the overall sample size for all events, especially the extreme events that are more likely to be detected with observations from multiple gauges distributed spatially across the region (Hayhoe et al., 2008; Hayhoe et al., 2007; Hoerling et al., 2016; Tebaldi et al., 2006).

Projections of future changes to AMT were obtained from the NASA Goddard Institute for Space Studies, Center for Climate Systems Research at Columbia University in New York City. Because this research was initiated prior to the release of the Coupled Model Intercomparison Project 5 (CMIP5) and the most recent CMIP6, neither the Representative Concentration Pathways (RCPs) of CMIP5 nor the Shared Socioeconomic Pathways of CMIP6 are referenced explicitly. Instead, the MIROC GCM (Hasumi & Emori, 2008) was selected for this analysis because its higher relative predicted increases in temperature would yield a more pronounced effect on the generated precipitation series. AMT projections under the A2 emission scenario, "a very heterogeneous world," (Nakicenovic et al., 2000) were used due to the regional scale of this study.

Following the procedure described in Yu et al. (2018), the continuous hourly pressure time series were discretized into individual pressure change events (PCEs) associated with fronts or other precipitation-causing systems. During the identification of PCEs, daily fluctuations in atmospheric pressure were minimized by defining the pressure change as the difference between two pressure readings separated from each other by 24 hr, as shown in Equation 1:

$$\Delta P_t = P_t - P_{t-24} \tag{1}$$

where P_t is the pressure reading at hour t, and ΔP_t is the pressure change relative to 24 hr prior. PCEs were categorized as either Increasing (InPCEs) or Decreasing (DePCEs) based on the computed direction of the pressure change.

Two important features defining the magnitude of each PCE are the duration and the Cumulative Event Pressure Change (CEPC). In the stochastic process described in the next section, these two features will be used as the conditions for selecting the subsequent PCE. The CEPC for each PCE is defined per Equation 2:

$$\text{CEPC} = \sum_{t=0}^{d} \Delta P_t \tag{2}$$

where ΔP_t is the 24-hr pressure change relative to hour t in a PCE defined in Equation 1, and d is the duration of the PCE. The intensity, duration, and alternate on of DePCEs and InPCEs correspond to the strength and speed of the precipitation causing meteorological systems as they move past the recording gauges.

3. Methodology

3.1. Algorithm Design

Yu et al. (2018) used PCEs to describe the relationship between AMT and specific precipitation characteristics, including the Probability of Precipitation (POP) and the event Precipitation Depth (PD). PCEs, and especially DePCEs, were shown to be associated with the vertical lifting of air and associated condensation, coalescence, and precipitation. The analysis also showed that the frequency of PCEs can be represented as a function of AMT, suggesting that a synthetic series of future PCEs can be derived from future AMT projections.
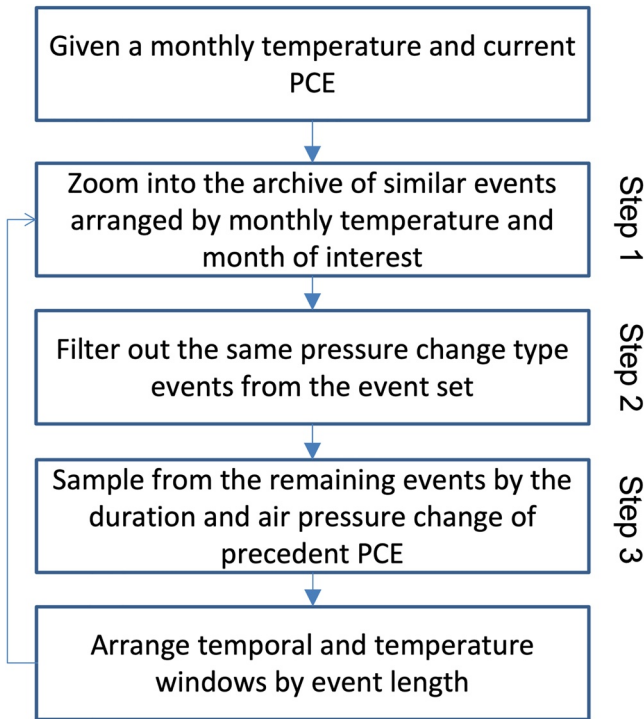
Figure 1. Flow chart of the synthetic precipitation generation algorithm.

The model uses nonparametric methods to simulate precipitation, making it portable to other regions (Basinger et al., 2010). The algorithm samples historical PCEs from specific AMT ranges (indexed to GCM outputs) occurring within moving time windows. Since the characteristics of PCEs (e.g., type and magnitude), their associated precipitation characteristics (e.g., POP and PD), and AMT are statistically and physically related (Yu et al., 2018), a synthetic precipitation series can be generated by concatenating precipitation event characteristics associated with specific sequences of PCEs. (Additional analysis regarding the relationship between POP and PCE is presented in Appendix A).

Figures 1 and 2 provide more detail on the procedure used to sample an individual PCE based on temperature and time. The overall stochastic algorithm is represented in Equations 3 and 4, where PCE_1 is selected from a group of candidate PCEs, {PCE}, that could begin at the time t_0 based on the GCM-projected AMT for t_0, (AMT_0), and the size of the moving window, Win. Specifically, the set {PCE} is selected based on Equation 3.

$$\{PCE\} = f(t_0, AMT_0, \text{Win}) \tag{3}$$

PCE_1, the new successive PCE, is selected from within {PCE} but is conditioned on the preceding PCE, PCE_0, in the sequence per Equation 4.

$$PCE_1 = f(PCE_0, \{PCE\}) \tag{4}$$

The moving window has been used to simulate temporally stationary precipitation by other researchers using different lengths, such as 60 days by (Sharma & Lall, 1999) or 90 days by (B. Rajagopalan & Lall, 1999). The decision to use a shorter window (e.g., 30 days) was made in this study to better represent seasonality. The seasonal window is further narrowed using temperature, such that only PCEs corresponding to a particular time of the year and temperature is selected, creating stability to the algorithm. The 6°C window was selected because seasonal shifts of POP for both DePCE and InPCE were detectable in this range (Yu et al., 2018). For example, in Figure 2, a day in March with AMT of 9°C can be used to select the subsequent PCE. The horizontally and vertically shaded bars, both centered at this data point, graphically depict the 30-day, and the 6°C, windows, respectively. The intersection of these two shaded bars defines the set {PCE}, described by Equation 3.

Steps 2 and 3 of Figure 1 can be denoted by Equation 4, where the new PCE will be sampled from {PCE} based on the condition of the previous one, PCE_0. In step 2, the PCEs of the same type of PCE_0 are excluded, ensuring that InPCEs are always followed by DePCEs and vice versa. In Step 3, a K Nearest Neighbor (KNN) approach (Lall & Sharma, 1996) is employed to select one PCE out of the remaining PCEs from Step 2 to append to the synthetic series after PCE_0. In this study, "nearest neighbors" are selected from {PCE} based on the magnitude of PCE_0, defined by the Euclidian distance of the standard scores of CEPC and event duration (Additional details provided in Appendix A). Specifically, the candidate PCE in {PCE} whose predecessor's magnitude is closest to the magnitude of PCE_0 will be chosen as the subsequent one to continue the generation.

After the selection of PCE_1, the time of interest is advanced from t_0 to t_1 by the duration of PCE_1 (Equation 5). Next, t_1 is used to update the projected AMT, AMT_1 in Equation 6. For example, if t_0 is 2054-1-31 10:00 and the duration of PCE_1 is 25 hr, then t_1 will be 2054-2-1 11:00. AMT_1 will be the AMT projected for Feb 2054.

$$t_1 = t_0 + \text{duration } of \ PCE_1 \tag{5}$$

$$AMT_1 = f(t_1) \tag{6}$$

After completing the stochastic process, the corresponding precipitation series of each synthetic PCE is concatenated to form the final hourly synthetic precipitation series.
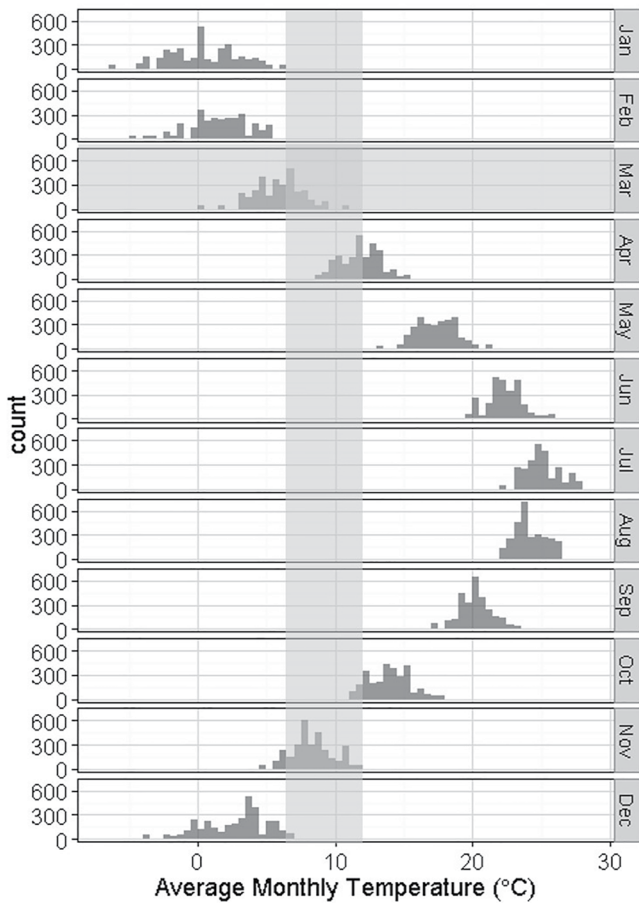
Figure 2. Sample of a two-dimensional moving window, a day in March with 9°C average monthly temperature is the time of interest. The horizontal shadow area is the 30-day moving window. The vertical shadow area is the 6°C wide temperature window, centered on 9°C. The pressure change events in the intersection are the candidates for sampling the next one.

3.2. Two-Step Validation Approach

To validate the approach, the algorithm was used to generate synthetic sequences of precipitation for both historic (e.g., 1975–2012) and future (e.g., 2035–2099) periods. One hundred realizations of precipitation for each of these time periods were generated. The stochastic process is only applied to generating the synthetic PCE series using the target AMT as the basis. The historic simulations were generated using observed AMT, while the future simulations used the climate change AMT projected by Center for Climate Systems Research at Columbia University. Precipitation records of each PCE based on their observational correspondence are then concatenated into the synthetic precipitation series in the order of the generated PCE series. To simplify the discussion, the time series of historic precipitation observation is referred to as the "Observed" series, the modeled time series of the historic period overlapping with the "Observed" is referred to as the "Reanalysis" series, and the modeled time series of the future period is referred to as the "Forecasted" series.

The validation process involves two steps. In step 1 (described in Section 4.1), the Reanalysis series is compared to the pooled precipitation observations described above, demonstrating the algorithm's ability to replicate the physical link between precipitation occurrence and temperature. The goal is to demonstrate the model's ability to bracket trends displayed in the historical data. This comparison will first depict the relationship between PD and the magnitude of pressure change (e.g., CEPC). Next, it will show the impact of temperature (e.g., AMT) and the dependence of different seasonal PD percentiles on temperature (e.g., AMT). The analysis of PD distributions in all the plots in the following sections are displayed in contours while the trends of PD are lined up by Loess regression curves (Cleveland et al., 1992) are generated to display trends in these relationships.

In Step 2 of the validation process (described in Section 4.2), the forecasted series are qualitatively compared to precipitation forecasts made for this period by Hayhoe et al. (2007). Box plots of seasonal and annual PD for 2035–2069 and for 2070–2099 are developed for comparison with box plots for the same future time slices generated by Hayhoe et al. (2007). This same plot is used to discuss the implications of climate change on future precipitation, specifically through a comparison of the Reanalysis series to the Forecasted series. A further breakdown of the shifts of distributions and trends of seasonal precipitation of the reanalysis series is presented against pressure change (e.g., CEPC) and temperature (e.g., AMT).

4. Results

4.1. Validation Step 1: Comparison of All Series

We note that because the Reanalysis series includes 100 replicates of the historic period, it more clearly presents the characteristics of PCE than the pooled observations. To reflect the relationship between precipitation and temperature, the results are presented for each of the three series.

The relationships between PD and CEPC embedded in all time periods are shown in Figure 3, with nearly identical trends evident in all series. Because all dry PCEs lie on the horizontal axis (e.g., PD = 0 mm), the contours reflect the density distribution of only the wet-weather PCEs. The contours show a nearly identical distribution of PCEs over all three series. On the horizontal axis, 0 hPa separates DePCEs (to the left) and InPCEs (to the right). This point on the horizontal axis also corresponds to a point of inflection in the PD trend line. The steeper slope of the PD trend line indicates that precipitation is more sensitive to DePCEs than to InPCEs. Among DePCEs, PD increases with increasing (negative) CEPC. Among InPCEs, PD decreases with increasing (positive) CEPC. These differences are not surprising because increasing pressure tends to be associated with increased atmospheric
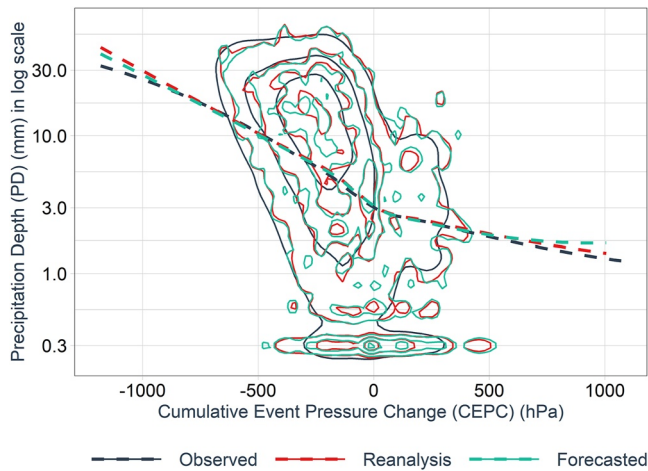
Figure 3. The relationship between Precipitation Depth (PD) and Cumulative Event Pressure Change (CEPC) of all pressure change events (PCEs) for the comparisons of Observed, Reanalysis (for validation), and Forecasted (for showing climate change impacts). Since contours indicate the distribution of PCEs qualitatively, their corresponding values are not shown. Loess regression curves in-dash are shown for each data set to denote the trend of PD against CEPC.

stability, indicating less convection, condensation, coalescence, and precipitation. Slight discrepancies in the trend lines are apparent at the left and right extremities. The differences between the Reanalysis trend and the Observed trend at the extreme DePCEs and InPCEs are likely due to the larger sample size of the synthetic series. The impact of climate change is evident through the higher trend line for the Forecasted series at the extreme InPCEs. An analysis of the associated POP is provided in Appendix A.

As reflected in Figure 4, most of the high wet InPCEs (high end of the tiled area) are of mild PD and occur more frequently in low AMT. With the spreading occurrence region toward warm AMT in the Forecasted for all categories, extreme wet InPCEs will have higher PD under the climate change, which agrees with the discrepancy of trend lines observed at the right end in Figure 3.

By introducing AMT and precipitation quantity as additional dimensions to the validation process, the distribution of PD can be further decomposed, as shown in Figure 4. Most precipitation events are categorized as mild PD (e.g., 0–20 mm) and, as a result, the distribution of PD is stable in the upper plot of Figure 4. Enhanced ensembles in the Reanalysis series provide a clearer transition from 5 to 10 mm than in the Observed.

For moderate events that have a smaller sample size, (e.g., PD = 20–60 mm) differences in the Observed and Reanalysis series distributions are more obvious. The contours of 35 mm retreat from the middle of the plot in the Reanalysis compared to the Observed. Only an isolated area located at 20°C and −300 hPa is denoted as >35 mm. Under the impacts of climate change in the Forecasted, the 35 mm contour retreats even further while the isolated peak area expanded toward low temperature and low CEPC.

Extreme events (e.g., PD > 60 mm) presented in the Observed series are too few and too scattered to discuss. In the Reanalysis series, the high DePCEs (low end of the tiled area) for all AMTs have PD > 100 mm. Impacts of climate change are evident in the Forecasted series as the region of PD > 100 mm extends to high AMTs. This observation is consistent with the projections of more extreme precipitation under climate change that have been made by many other researchers (Betts et al., 2007; Hamlet & Lettenmaier, 1999; Huntington, 2003; Labat et al., 2004), to be discussed further in the next section.

Additional insights of the dependence between PD and temperature can be derived from PD percentiles separated by type of PCEs (Figure 5). While the PD of DePCE is similar across all temperatures, the PD of InPCE generally increases with temperature, especially between 25th and 99th percentiles. This relationship could be related to the type of precipitations in different seasons. During winter, most weather mechanisms are systematic and the movement of the precipitation region is geographically related to DePCE. Once the shifting to InPCE, precipitation will end quickly causing PD of InPCE much lower than that of DePCE. But in summer, there are many localized convections that a rainy system generated in a DePCE of small geographic scale has a big chance to move into a large scale InPCE area remaining a big portion of PD. Specifically, DePCE is the small center forming precipitation while InPCE is the surrounding contributor of air and humidity. To balance a DePCE, air must move downward in the surrounding region, creating an InPCE. However, the precipitation formation cloud is dynamically developed and moves. Given the tributary InPCE area is usually much larger than what can be represented by the point-sourced data collected at ground-based stations, precipitation was more difficult to be observed for InPCEs than for DePCEs, especially in local systems in summer. In addition to PD, the variance of PD percentiles of InPCE expands as the temperature gets warm, indicating that such possibility may get higher at extreme PD. The relationship between POP with seasonality and for different PCE types is explored in Appendix A.

4.2. Validation Step 2: Comparison of the Forecasted Series to Forecasts Made by Others

In this section, the SPG algorithm results will be qualitatively compared to other research. After researching nine coupled atmosphere-ocean general circulation models (AOGCMs) under different emission scenarios, Hayhoe et al. (2007) projected a consistent change of precipitation under global warming across the Northeast United
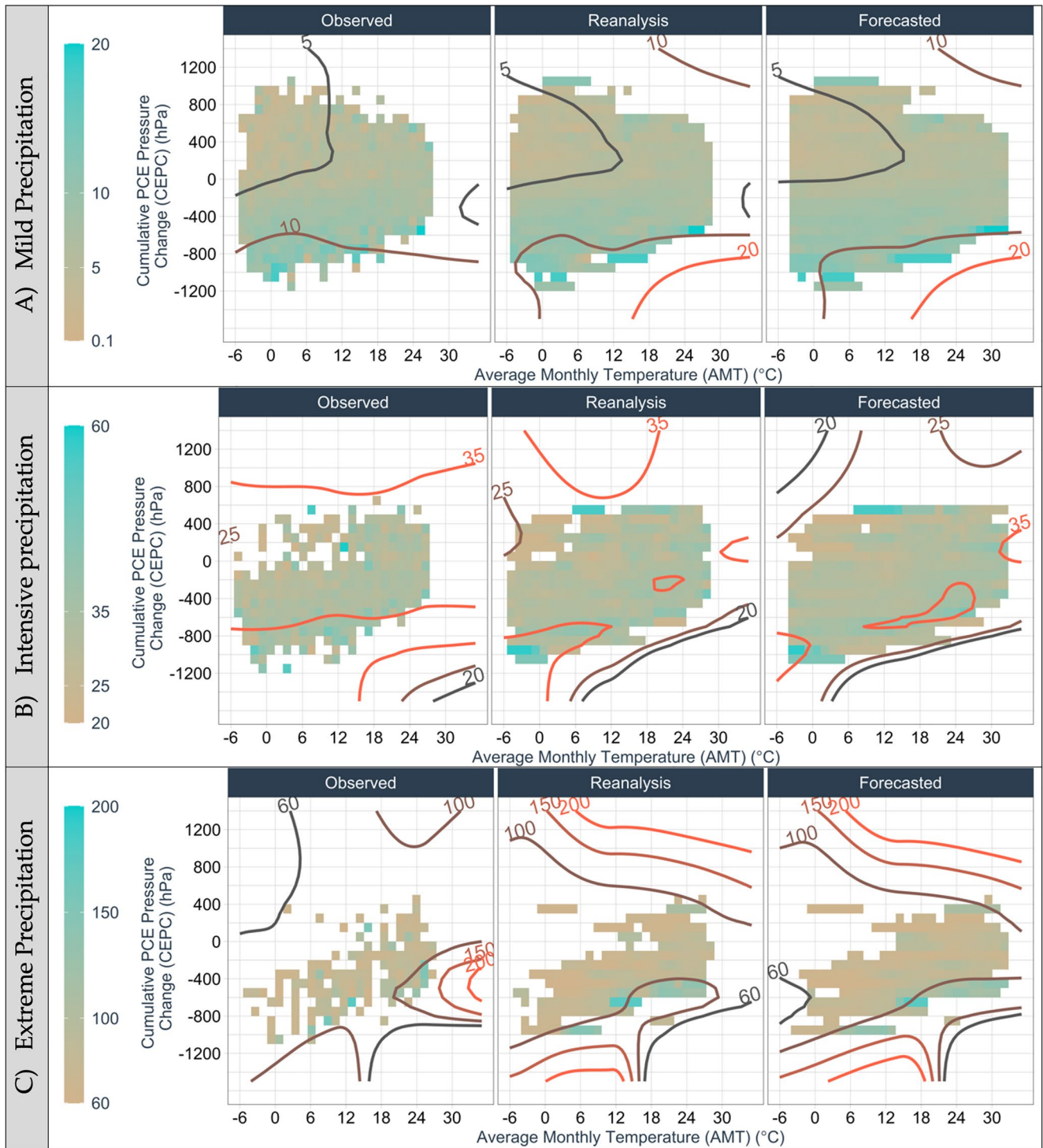
Figure 4. Relationship of Precipitation Depth (PD) against Cumulative Event Pressure Change (CEPC) and Average Monthly Temperature (AMT) in different ranges of PD. The color area represents the average PD of rainy pressure change events corresponding to different combinations of CEPC and AMT. Contours and labels indicate the local regressions of PD versus CEPC and AMT generated by the locfit function in R. (A: mild precipitation with PD between 0 and 20 mm, (b) moderate precipitation with PD between 20 and 60 mm, and (c) extreme precipitation with PD > 60 mm).
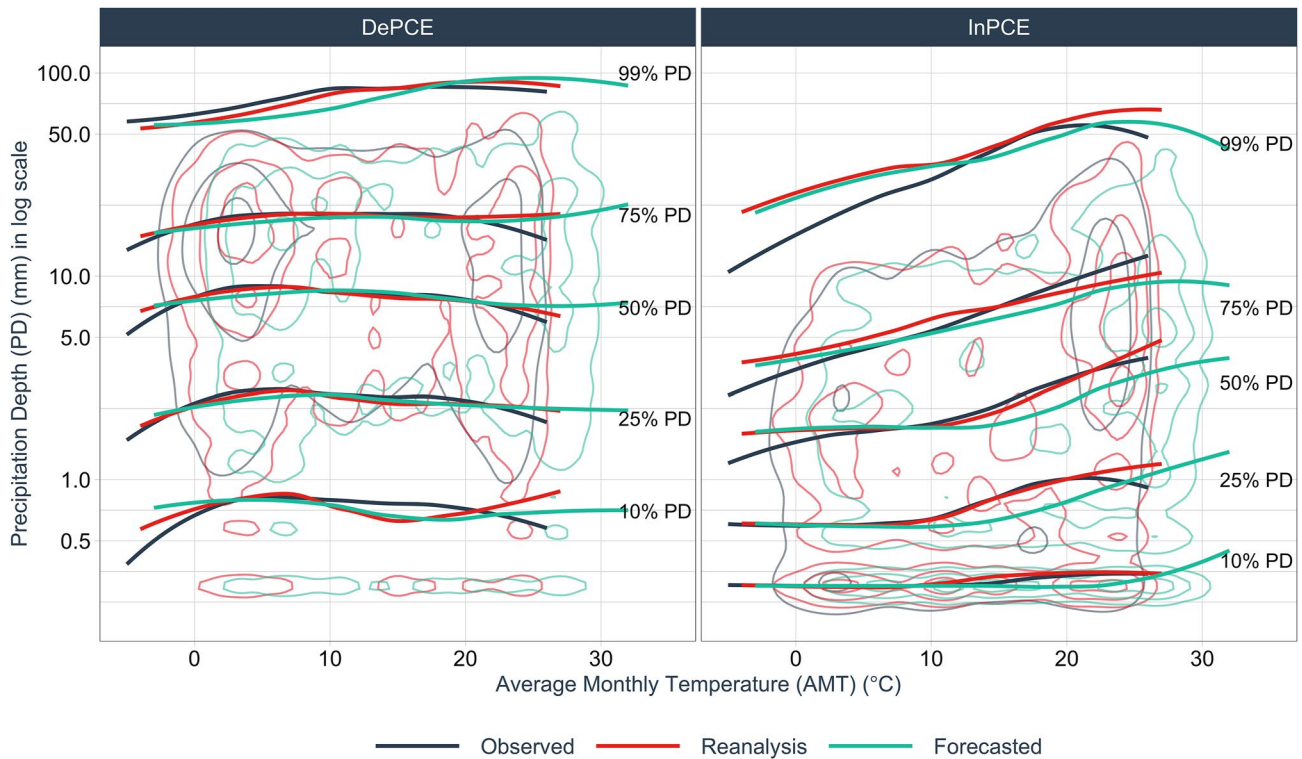
Figure 5. Dependence of pressure change event (PCE) type and Precipitation Depth (PD) on Average Monthly Temperature (AMT). The contours represent the distributions of PCE in different data sets. Again, since contours indicate the distribution of PCEs qualitatively, their corresponding values are not shown. The percentiles of PD illustrate its trend and variances against AMT.

States, with the magnitudes positively correlated to GHG emissions. As shown in Figure 6a, under the A2 emissions scenario, annual temperature and precipitation across the Northeast United States are projected to increase by about 2.5°C and 6%, respectively during 2035–2064 and by about 4.5°C and 8% during 2070–2099, respectively. The greatest percent increase in precipitation is expected to occur in winter.

Figure 6b presents a seasonal comparison of temperature and precipitation change between the Observed and the Forecasted data sets for the two time slices considered in Hayhoe et al. (2007). AMT projections show a gradual increase of about 2°C by 2069 and 5°C by 2099 on average, annually as well as for both summer and winter. The modeled change in precipitation reflects a shift that partially aligns with the projections by Hayhoe et al. (2007). While annual increases are small and hard to differentiate, winter precipitation will increase more both before and after the 2069 breakpoint than Hayhoe et al. (2007). Summer precipitation will decrease by about 5% in the two future time slices. These findings qualitatively agree with the projections by Hayhoe et al. (2007), validating the results.

Figure 7 provides a closer examination of the seasonal trends of PD relative to CEPC and AMT and reveals more information about precipitation changes under climate change by focusing on three time periods, the observed period, 2035–2069, and 2070–2099. According to Yu et al. (2018), maximum PCE frequencies occur at 0°C. This observation suggests that global warming may promote atmospheric stability, producing more PCEs for small CEPCs. This phenomenon can be observed from the upward trend of PCE distributions from the observed period to 2035–2069 and to 2070–2099 in Figure 7, especially in winter, spring, and fall. For summer, although the upward trend is not pronounced, the portion of PCE distributions (solid lines) <10 mm (dashed lines) shrinks from the observed period to 2035–2069 and to 2070–2099, indicating that small PD will be less frequent in the climate change impact. This could be due to the reason that the convection system in summer is much more intensive than in other seasons and can deplete the amplified moisture-holding in warmer air under the CC relationship. However, the portion of the rainy PCEs in summer (labeled under the marginal density plot) out of all rainy PCEs indicates that the chance of summer precipitation will slightly decrease from 24.7% to 24.6%. Thus, even though intensive PD would be favored under warm AMT, the overall summer PD may not increase, agreeing
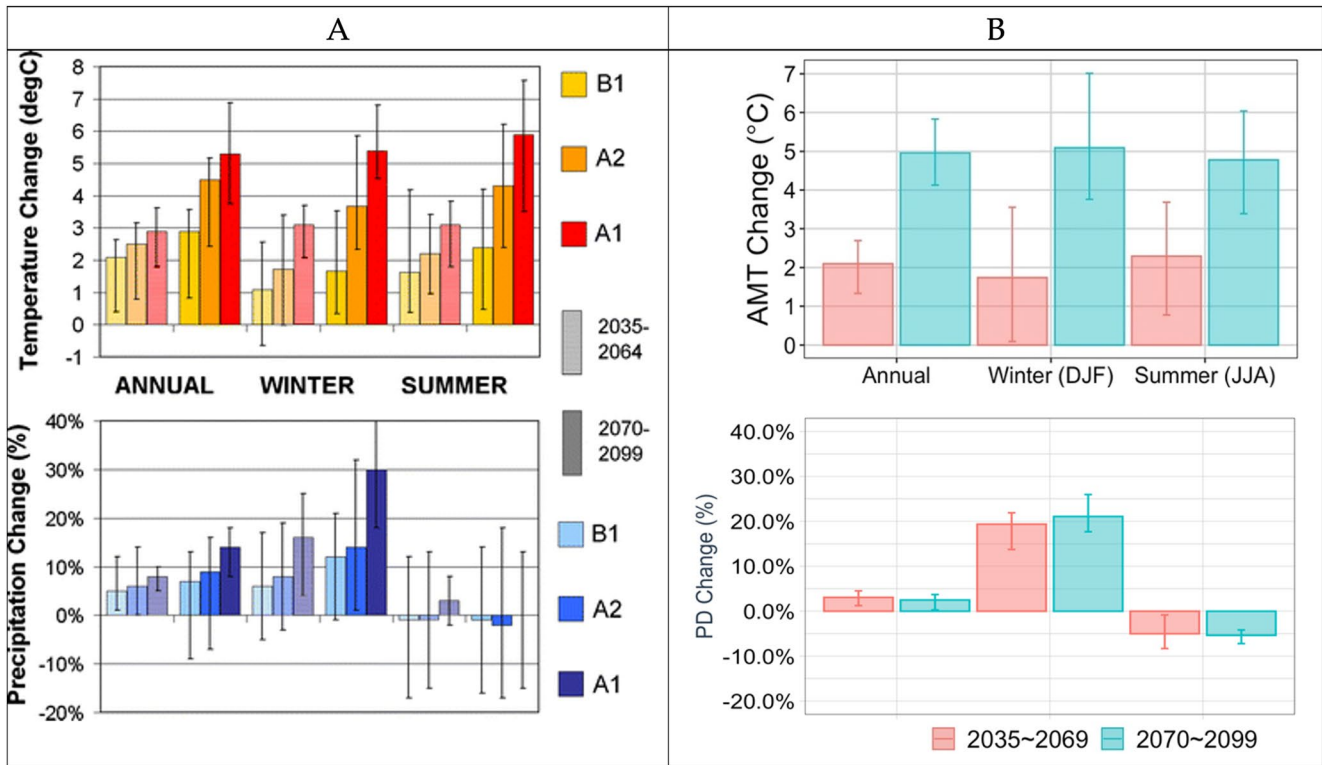
Figure 6. Comparison of temperature and precipitation projections in NE United States in A2 emissions (A from (Hayhoe et al., 2007) and B from the Observed and the Forecasted data sets).

with Figure 6. In winter, the portion of rainy PCE will increase from 26.1% to 26.7% during 2035%–2069% and to 27.3% during 2070–2099. Consequently, an increase in winter PD would occur as Figure 6 shows.

5. Key Findings

The foundations of this algorithm are the relationships between precipitation and AMT using PCE characteristics as a medium for interpreting the precipitation mechanism. With the logic that precipitation is subject to its PCE characteristics while the PCE occurrence is determined by temperature (AMT → PCE → Precipitation), synthetic future precipitation time series were created using AMT as a primary input for generating PCE sequence under climate change. It is crucial that the algorithm has a sound physical basis because (a) the physical construct should not vary significantly as the climate changes and (b) empirical models may not be valid or accurate when extrapolated beyond observed data sets.

Many researchers have endeavored to describe the dependency of precipitation on temperature, such as prior and post temperature change to an extreme precipitation event in a tropical area (Visser et al., 2020). As atmospheric instability favors precipitation formation, high CEPC is an indicator for vertical air movement, condensation, and precipitation and as such is representative of the CC relationship. Therefore, extreme events (e.g., summer convections and winter blizzards) with intensive precipitation formation mechanisms have the capability to deplete the precipitable moisture. The trend is apparent in InPCE as indicated by PD driven percentiles shown in Figure 5. As intensive and rainy InPCE are typically contributory to intensive DePCE, the CC relationship is an accurate representation of these conditions.

Figure 5 reveals that the PCE type plays an important role. Condensation is favored during DePCEs, the intensity of which indicates the forces extracting moisture from the air. This could be a possible explanation for the stable distribution of PD over the temperature in Figure 5. At the same time, strong air convection requires the intake of air from surrounding regions that are much larger than the rainy zone itself. In other words, a high-intensity DePCE is balanced by a high-intensity wide-spreading InPCE. Thus, precipitation during InPCEs usually occurs
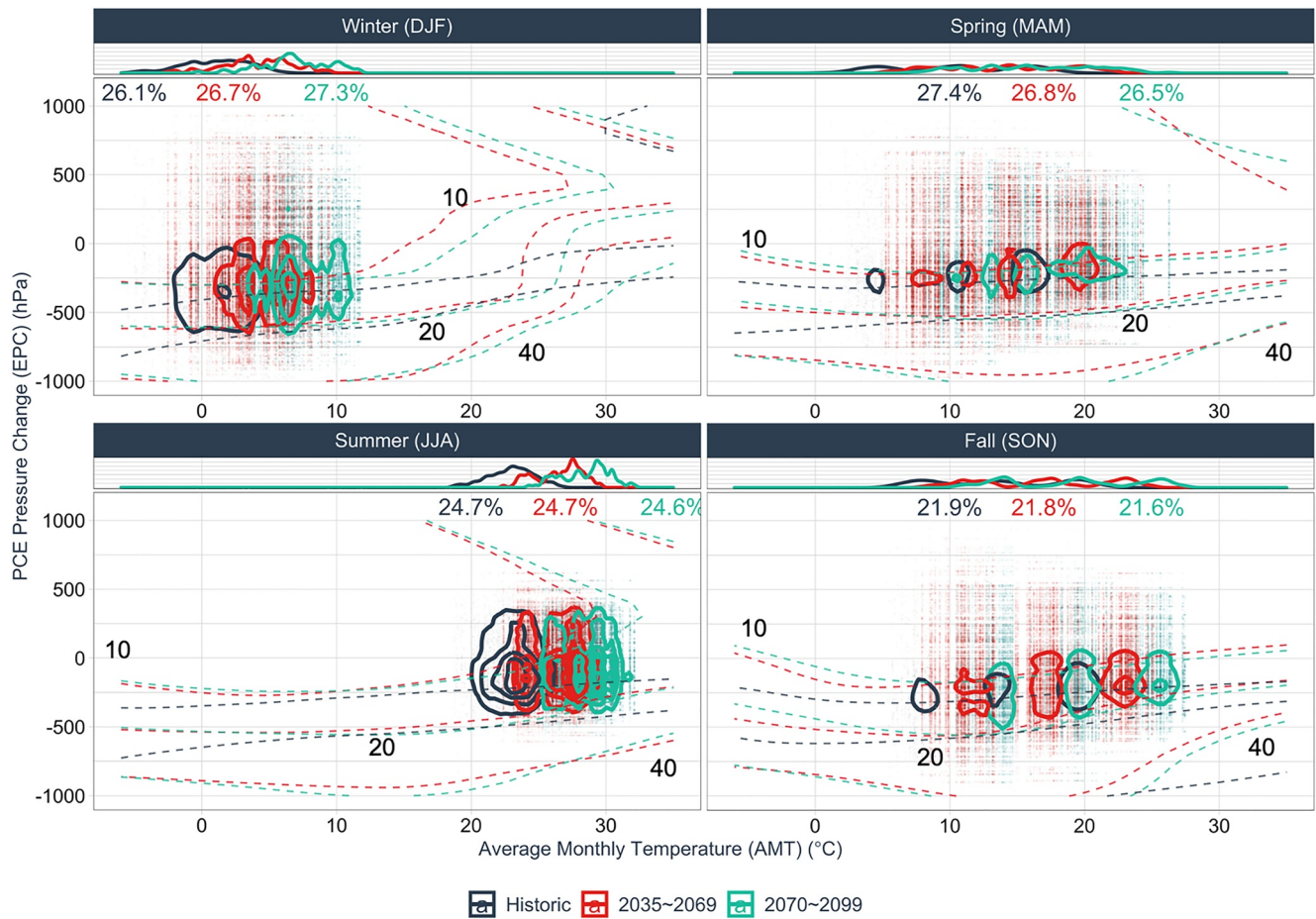
Figure 7. Seasonal average Precipitation Depth (PD) change versus Cumulative Event Pressure Change (CEPC) and Average Monthly Temperature (AMT) in the Observed data set and different projection periods. Solid contours represent the main distribution of pressure change events (PCEs), while the dotted lines show the distribution of PD. Again, since contours indicate the distribution of PCEs qualitatively, their corresponding values are not shown. Dotted contours and labels in black are in millimeters indicating the local regression of PD versus CEPC and AMT generated by the locfit function in R. The percentage numbers below the marginal density plots show the portion of PCEs of each season in a year for different data sets.

when the observation site is originally outside of the core DePCE area but located on the path of the rainy zone movement. Consequently, not all available moistures can be condensed, and this condition is even capped by the moisture-holding capacity represented by the shift up of PD distribution for InPCE in Figure 5. The analysis also shows that during InPCEs, PD increases above 12°C in Figure 5, likely corresponding with the increased frequency of thunderstorms and other severe air convection beginning in spring and agreeing with condensed summer PD contours in Figure 7.

The dissimilarities observed in intensive CEPC PD in Figure 3 suggest that extreme PD is likely to become more intensive in the future as the temperature warms. Given that summer DePCEs are likely to skew toward non-high-intensity events (see Figure 7), intensive DePCEs (−2000 to −300 hPa) that cause extreme precipitation are likely to occur less frequently. Accounting for warming, the remaining extreme precipitation associated with intensive DePCEs would be benefited from the CC relationship and result in more severe precipitation stress in the future.

6. Limitations and Future Efforts

One of the main purposes of this study was to demonstrate the physical soundness of PCE as a medium to associate precipitation and temperature. Thus, the study did not include many climate models to obtain a robust sample size for analysis and the analysis was not conducted statistically. We believe that the physical phenome-

non represented by PCE will be generally found in any climate model but MIROC, the extreme condition, could embody it more pronouncedly than other mild models.

Although the results qualitatively agree with other research, the current algorithm resamples observed events without altering their volumes or temporal patterns whose changes are expected under global warming (Fadhel et al., 2018; Wasko & Sharma, 2015). Although better extrapolation of future precipitation can be made, introducing scaling parameters, however, may bring bias to the demonstration of this algorithm. Being conservative in this study to prove the physical soundness of PCE as the first step, our future work will focus on how to tune the model or scaling for extrapolation.

In addition, the hourly time step was not fine enough to reflect the temporal pattern of a precipitation event, especially in summer convections. To solve this issue, possible improvements could be the following: (a) using new data in more granular temporal scales to embody the patterns of extreme weather events, (b) investigating the nexus of temperature, humidity, and pressure in triggering and producing precipitation, and (c) quantifying the scaling impact of climate change on the volume and temporal patterns of PCEs, which is the driven force of moisture extraction. A recent study has been published for the second option to investigate the associations among precipitation, PCE, and absolute humidity using data from Florida, United States. It reveals that the pattern of absolute humidity responding to precipitation varies on CEPC and season jointly (Zhang et al., 2022).

In contrast to precipitation, the above improvements can also be applied to drought since InPCE is very likely an important indicator of no rain. More importantly, PCE brings the information to preserve the physical concepts that hold regardless of location, time, and weather conditions while generating synthetic series. Once weather conditions can be classified properly by including PCE with other weather variables, the PCEs observed from a larger geographical scale can be gathered to better represent the true concept. The significantly enhanced sample size may result in a larger matching range of CEPC for the trend lines in Figure 3 and mitigate the tail discrepancies. Such improvement may support the current nonparametric algorithm for any location and more severe projected climate change temperature in the physical system represented by this large geographical area.

7. Summary and Conclusion

A nonparametric stochastic algorithm for generating nonstationary hourly precipitation was developed. The semiphysical link between hourly precipitation and Average Monthly Temperature (AMT) was built using PCE. Moving windows on both temperature and time were used to identify PCE and associated historical hourly rainfall observations that could be used to simulate future changing conditions. A multivariate bootstrapping method was employed to reflect the covariance of Cumulative Event Pressure Change (CEPC) and PCE duration in a simulation process. This process is a very important finding that provides a sophisticated solution to build the relationship between global climate model (GCM) temperature projections on a coarser temporal scale and climate characteristics on a finer scale.

After applying GCM AMT projections for the US Northeast until 2099, this algorithm was used to generate synthetic PCE ensembles and associated precipitation series qualitatively agreeing with the projections obtained by other researchers in terms of seasonal precipitation and extreme precipitation. Precipitation Depth (PD) was found to be strongly correlated to PCE. The PCEs can be used to link temperature and precipitation dynamics, presenting a more physically plausible concept, in contrast to pure statistical assumptions used by most existing models.

Overall, the analysis suggests the following:

- Increasing Pressure Change Event (InPCE) PD increases with AMT more significantly than with Decreasing Pressure Change Event (DePCE), which could be due to the point sourced data in this study
- In the NE United States, more frequent mild and lighter precipitation events are likely to occur in the future during all seasons
- Overall, summer precipitation is likely to be reduced, while summer extreme events are likely to become more frequent under climate change
- Winter precipitation is likely to increase

Moreover, because PCEs are more strongly related to precipitation formation than coarser temporal scale temperature (e.g., monthly), this algorithm may represent a reliable method for downscaling precipitation from GCM

AMT projections, which are more trustworthy than GCM precipitation projections on their own. Despite being nonparametrically structured, PCE could also be further explored as a means of integrating physically plausible synthetic future events into time series generated, even through parametric procedures.

In conclusion, this paper demonstrates a means of generating long, continuous, and synthetic precipitation series scaled-down from GCM AMT projections. These series could then be used for a variety of climate change model applications, such as hydrologic and hydraulic modeling, water resource modeling, and agriculture applications, etc.

Appendix A

A1. Geographic Scope

The model in this study is developed based on historical weather observations from three big cities, Philadelphia, New York City, and Boston (See Figure A1), to represent the weather conditions in the Northeastern coastal United States.

A2. Dependence of Precipitation on PCE Characteristics

The CEPC magnitude and PCE duration are used in the KNN analysis because of their relationships to the stability of air masses. Since a collision of air mass is usually accompanied by pressure change, the PCE duration is considered a general indicator of the horizontal stability of the air mass over the weather station (i.e., a short PCE indicates a stable air system). Within an air mass, vertical stability is negatively associated with CEPC magnitude. For example, the smaller the CEPC, either DePCE or InPCE, the more vertically stable the air mass and vice versa. Precipitation is more likely to form in vertically unstable air masses (Ackerman & Knox, 2007; Ackerman & Knox, 2015), especially DePCE.
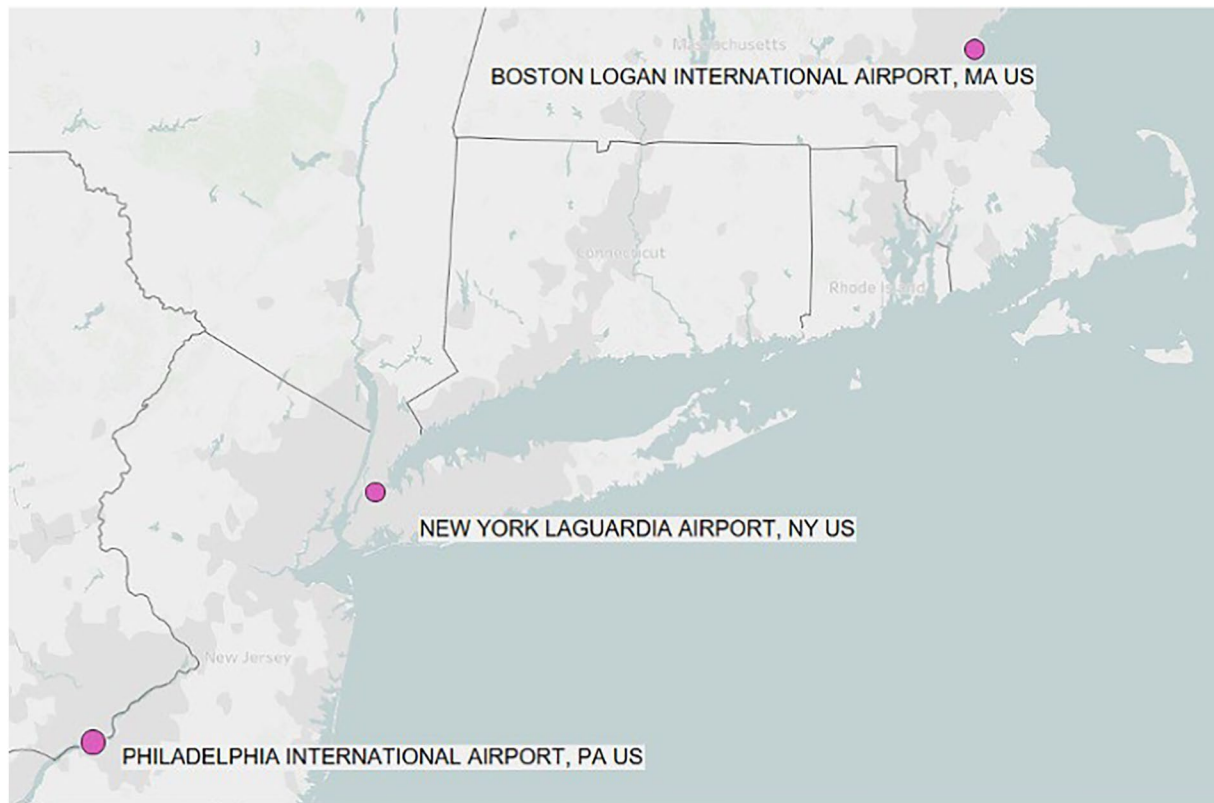

Figure A1. Locations of weather stations in the research area (size of circles indicates the length of available data) New York City (station ID: 72503014732 for 1973–2018 and 99999914732 for 1948–1973), Philadelphia (station ID: 72408013739 for 1973–2018 and 99999913739 for 1941–1973), and Boston (station ID: 72509014739 for 1943–2018) from NOAA NCEI (https://www.ncei.noaa.gov/access/search/index).
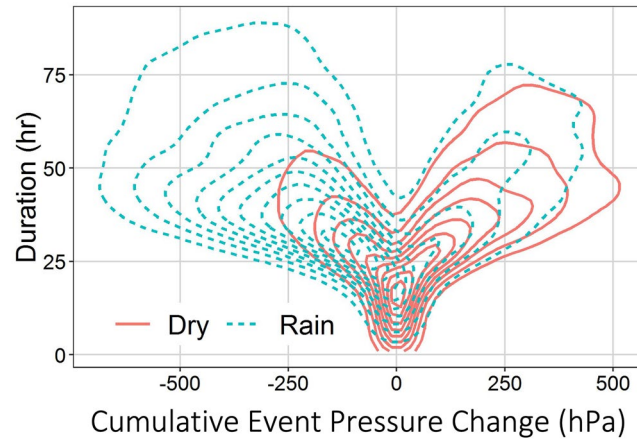
Figure A2. Precipitation dependence on both pressure change event (PCE) duration and Cumulative Event Pressure Change (CEPC) (Red: dry PCE and Blue: wet PCE).

For illustration, Figure A2 graphically depicts the relationship between CEPC and PCE duration of all historical PCEs. The contours indicate that precipitation is more likely to occur during DePCE, favored by both intensity and duration.

To consider both CEPC and duration of the stochastic process, the magnitude of a PCE is defined by Equation A1.

$$M_{\text{PCE}} = \sqrt{(d_z)^2 + (CEPC_z)^2} \tag{A1}$$

where M_{PCE} is the magnitude of a PCE; subscript z denotes the z score of the corresponding data set; and d_z and $CEPC_z$ are the z scores of the duration and CEPC of the PCE, respectively. The conversion of the z score helps obtain equal weighting for the two features in determining the magnitude of a PCE.

A3. K Nearest Neighbor (KNN) Parameter Selection

In Step 3 of the algorithm (Figure 1), the measure to determine the "nearest neighbors" is calculated by the Euclidian distance integrating both CEPC and PCE duration after scaling on the whole population. The value k is defined in the following equation suggested by Lall and Sharma (1996) on Page 684.

$$k = \sqrt{n}$$

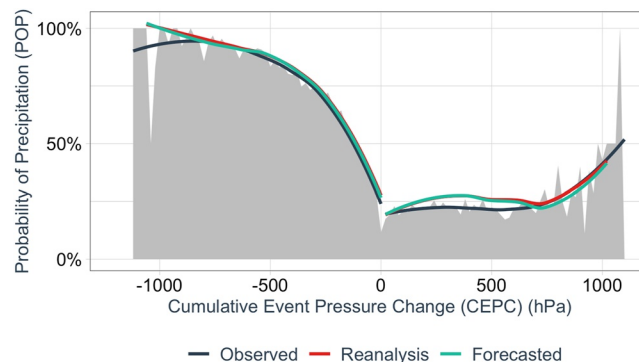where n is the number of PCE in {PCE}.

Figure A3. Dependence of Probability of Precipitation on Cumulative Event Pressure Change (CEPC). The gray area represents the Observed data. All data sets are fitted by Loess regression in different colors separated by two types of pressure change event at CEPC = 0 hPa.

A4. Relationship Between POP and CEPC

In Figure A3, as the magnitude of CEPC increases, the POP of DePCE climbs from 15% to 100% within 0–800 hPa, while InPCE POP increases only from 15% to about 50% within 0–1000 hPa. Given the limited sample size of extreme InPCE ($n = 79$ when CEPC >820 hPa in historical data), less confidence is associated with the POP beyond 820 hPa. For CEPC < −1000, there are five historical PCE observed in BOS between 1944 and 1946 without precipitation. But all of them have a sudden air pressure drop about 100 hPa within 1 hr, which lead to a heavy bias. Although these events are excluded in the analysis in our model, we treat the POP in this range as 100% regardless of the decreasing trend lines. Thus, falling pressure appears to be a better indicator of precipitation than increasing pressure.

In Figure A4, the POP in spring for DePCE historically oscillates between 50% and 70% with a low end at around 19°C. Despite the decrease beyond 15°C, its synthetic trend bears a similar general level. As for InPCE, POP remains around 25% for both the Observed and the Forecasted. The Forecasted POP trend on AMT spans a larger range than the Observed with a similar pattern after 5°C. This situation could also be found similar in summer and fall for both PCE types. Despite similar patterns, the winter POP of both PCE types historically increases after 6°C while the Forecasted series remain stable. This indicates that the rain likelihood would be lowered for warm winters in the future in this region. Focusing on the low variation parts in the middle-temperature range of all seasons, the POPs for both PCE types generally match between the Observed and the Forecasted.
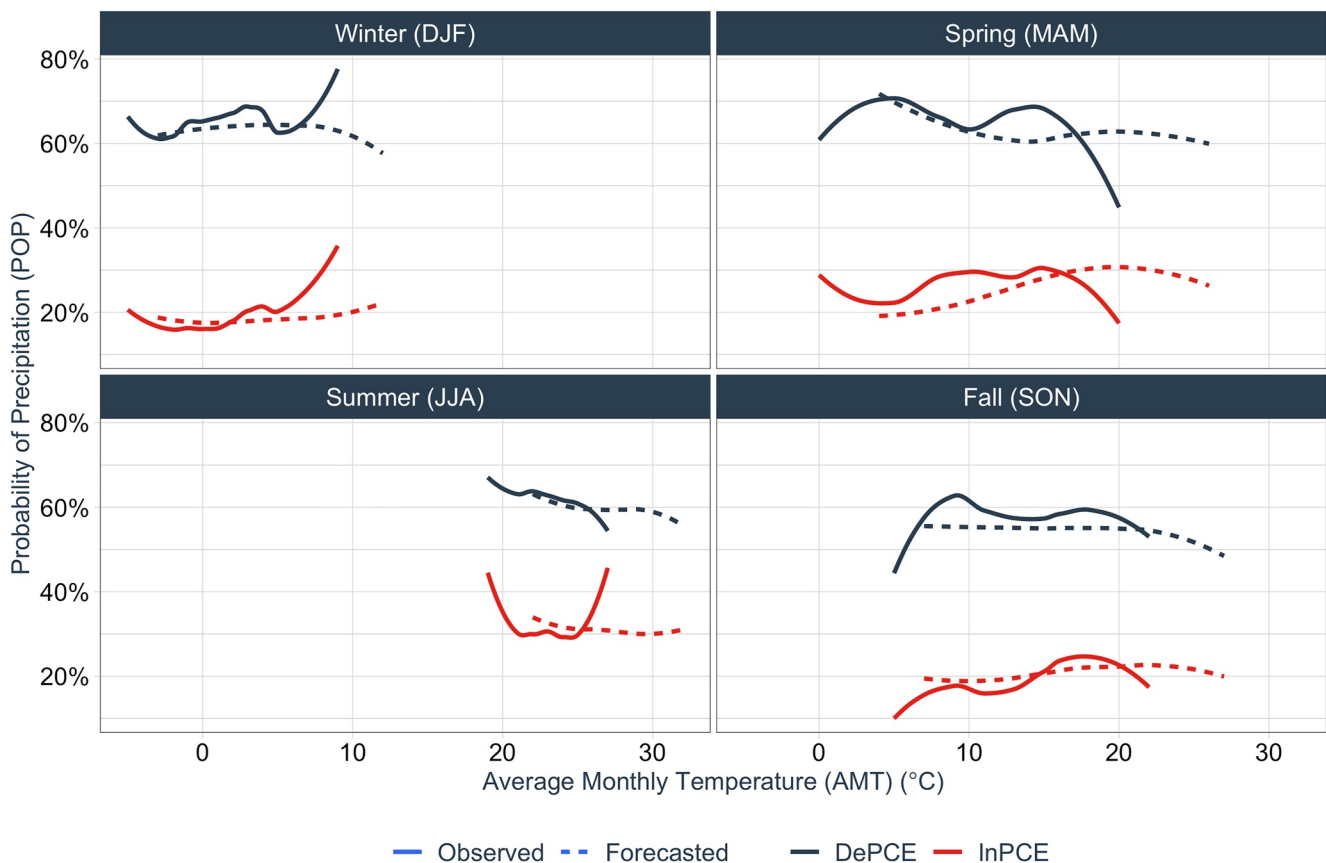

Figure A4. Seasonal dependence of Probability of Precipitation (POP) on Average Monthly Temperature (AMT). The average POP for each AMT from the Observed and the Forecasted data sets is differentiated by solid lines and dotted lines. Pressure change event types are colored differently.

A Glossary of Acronyms

AMT	Average Monthly Temperature
AOGCM	Atmosphere-ocean general circulation models
BOS	Boston
CC	Clausius-Clapeyron
CEPC	Cumulative Event Pressure Change for a single pressure change event
CMIP5	Coupled Model Intercomparison Project 5
CSO	Combined Sewer Overflow
DePCE	Decreasing Pressure Change Event
Forecasted	The data set of 100 synthetic replications of climate projection of 2035–2099
GCM	Global Climate Model
GHG	Greenhouse Gas
GI	Green Infrastructure
InPCE	Increasing Pressure Change Event
KNN	K Nearest Neighbor
NCDC	National Climate Data Center
NCEI	National Center for Environmental Information
NYC	New York City
Observed	The data set of historical observations
PCE	Pressure Change Event
PD	Precipitation Depth during a PCE
PHL	Philadelphia
POP	Probability of Precipitation
RCM	Regional Climate Model
RCP	Representative Concentration Pathway
SPG	Stochastic Precipitation Generator
Reanalysis	The data set of 100 synthetic replications of 1975–2012
Win	The size of the moving window including both time and AMT dimensions

Data Availability Statement

The data used in this study were obtained from National Center for Environmental Information (NCEI) at https://www.ncei.noaa.gov/access/search/index.

References

Ackerman, S. A., & Knox, J. (2015). *Meteorology: Understanding the atmosphere*. Jones & Bartlett Learning. Retrieved from https://books.google.com/books?id=PhjmnQEACAAJ

Ackerman, S. A., & Knox, J. A. (2007). *Meteorology: Understanding the atmosphere*. Thomson Brooks/Cole. Retrieved from https://books.google.com/books?id=qrcRAQAAIAAJ

Ahrens, C. D., Jackson, P. L., Jackson, C. E. J., & Jackson, C. E. O. (2012). Meteorology today: An introduction to weather, climate, and the environment. Nelson Education. Retrieved from https://books.google.com/books?id=jvnQiFG3dPkC

Allen, M. R., & Ingram, W. J. (2002). Constraints on future changes in climate and the hydrologic cycle. *Nature*, *419*(6903), 228–232. https://doi.org/10.1038/nature01092

Basinger, M., Montalto, F., & Lall, U. (2010). A rainwater harvesting system reliability model based on nonparametric stochastic rainfall generator. *Journal of Hydrology*, *392*(3–4), 105–118. https://doi.org/10.1016/j.jhydrol.2010.07.039

Betts, R. A., Boucher, O., Collins, M., Cox, P. M., Falloon, P. D., Gedney, N., et al. (2007). Projected increase in continental runoff due to plant responses to increasing carbon dioxide. *Nature*, *448*(7157), 1037–1041. https://doi.org/10.1038/nature06045

Cleveland, W., Grosse, E., & Shyu, W. (1992). Local regression models. In S. J. M. Chambers & T. J. Hastie (Eds.). Wadsworth & Brooks/Cole. Chapter 8 in Statistical models. 608p.

Evans, J. P., & Westra, S. (2012). Investigating the mechanisms of diurnal rainfall variability using a regional climate model. *Journal of Climate*, *25*(20), 7232–7247. https://doi.org/10.1175/jcli-d-11-00616.1

Fadhel, S., Rico-Ramirez, M. A., & Han, D. (2018). Sensitivity of peak flow to the change of rainfall temporal pattern due to warmer climate. *Journal of Hydrology*, *560*, 546–559. https://doi.org/10.1016/j.jhydrol.2018.03.041

Fowler, H. J., Blenkinsop, S., & Tebaldi, C. (2007). Linking climate change modelling to impacts studies: Recent advances in downscaling techniques for hydrological modelling. *International Journal of Climatology*, *27*(12), 1547–1578. https://doi.org/10.1002/joc.1556

Gill, S. E., Handley, J. F., Ennos, A. R., & Pauleit, S. (2007). Adapting cities for climate change: The role of the green infrastructure. *Built Environment*, *33*(1), 115–133. https://doi.org/10.2148/benv.33.1.115

Groisman, P. Y., Knight, R. W., Easterling, D. R., Karl, T. R., Hegerl, G. C., & Razuvaev, V. N. (2005). Trends in intense precipitation in the climate record. *Journal of Climate*, *18*(9), 1326–1350. https://doi.org/10.1175/jcli3339.1

Haberlandt, U., von Eschenbach, A. D. E., & Buchwald, I. (2008). A space-time hybrid hourly rainfall model for derived flood frequency analysis. *Hydrology and Earth System Sciences*, *12*(6), 1353–1367. https://doi.org/10.5194/hess-12-1353-2008

Hamlet, A. F., & Lettenmaier, D. P. (1999). Effects of climate change on hydrology and water resources in the Columbia River basin. *Journal of the American Water Resources Association*, *35*(6), 1597–1623. https://doi.org/10.1111/j.1752-1688.1999.tb04240.x

Hasumi, H., & Emori, S. (2008). K-1 Coupled GCM (MIROC) Description K-1 model developers.

Hayhoe, K., Wake, C., Anderson, B., Liang, X. Z., Maurer, E., Zhu, J. H., et al. (2008). Regional climate change projections for the Northeast USA. *Mitigation and Adaptation Strategies for Global Change*, *13*(5–6), 425–436. https://doi.org/10.1007/s11027-007-9133-2

Hayhoe, K., Wake, C. P., Huntington, T. G., Luo, L., Schwartz, M. D., Sheffield, J., et al. (2007). Past and future changes in climate and hydrological indicators in the US Northeast. *Climate Dynamics*, *28*(4), 381–407. https://doi.org/10.1007/s00382-006-0187-8

Heneker, T. M., Lambert, M. F., & Kuczera, G. (2001). A point rainfall model for risk-based design. *Journal of Hydrology*, *247*(1), 54–71. https://doi.org/10.1016/S0022-1694(01)00361-4

Hoerling, M., Eischeid, J., Perlwitz, J., Quan, X.-W., Wolter, K., & Cheng, L. (2016). Characterizing recent trends in US Heavy precipitation. *Journal of Climate*, *29*(7), 2313–2332. https://doi.org/10.1175/jcli-d-15-0441.1

Hoxit, L. R., Chappell, C. F., & Fritsch, J. M. (1976). Formation of mesolows or pressure troughs in advance of cumulonimbus clouds. *Monthly Weather Review*, *104*(11), 1419–1428. https://doi.org/10.1175/1520-0493(1976)104<1419:FOMOPT>2.0.CO;2

Huntington, T. G. (2003). Climate warming could reduce runoff significantly in New England, USA. *Agricultural and Forest Meteorology*, *117*(3–4), 193–201. https://doi.org/10.1016/s0168-1923(03)00063-7

Johnson, F., & Sharma, A. (2009). Measurement of GCM skill in predicting variables relevant for hydroclimatological assessments. *Journal of Climate*, *22*(16), 4373–4382. https://doi.org/10.1175/2009jcli2681.1

Johnson, F., & Sharma, A. (2012). A nesting model for bias correction of variability at multiple time scales in general circulation model precipitation simulations. *Water Resources Research*, *48*(1). https://doi.org/10.1029/2011WR010464

Kendon, E. J., Rowell, D. P., Jones, R. G., & Buonomo, E. (2008). Robustness of future changes in local precipitation extremes. *Journal of Climate*, *21*(17), 4280–4297. https://doi.org/10.1175/2008jcli2082.1

Kim, S., Eghdamirad, S., Sharma, A., & Kim, J. H. (2020). Quantification of uncertainty in projections of extreme daily precipitation. *Earth and Space Science*, *7*(8), e2019EA001052. https://doi.org/10.1029/2019EA001052

King, A. D., Klingaman, N. P., Alexander, L. V., Donat, M. G., Jourdain, N. C., & Maher, P. (2014). Extreme rainfall variability in Australia: Patterns, drivers, and predictability. *Journal of Climate*, *27*(15), 6035–6050. https://doi.org/10.1175/jcli-d-13-00715.1

Kunkel, K. E., Karl, T. R., Brooks, H., Kossin, J., Lawrimore, J. H., Arndt, D., et al. (2013). Monitoring and understanding trends in extreme storms: State of knowledge. *Bulletin of the American Meteorological Society*, *94*(4), 499–514. https://doi.org/10.1175/bams-d-11-00262.1

Labat, D., Goddéris, Y., Probst, J. L., & Guyot, J. L. (2004). Evidence for global runoff increase related to climate warming. *Advances in Water Resources*, *27*(6), 631–642. https://doi.org/10.1016/j.advwatres.2004.02.020

Lall, U., Rajagopalan, B., & Tarboton, D. G. (1996). A nonparametric wet/dry spell model for resampling daily precipitation. *Water Resources Research*, *32*(9), 2803–2823. https://doi.org/10.1029/96wr00565

Lall, U., & Sharma, A. (1996). A nearest neighbor bootstrap for resampling hydrologic time series. *Water Resources Research*, *32*(3), 679–693. https://doi.org/10.1029/95wr02966

Lenderink, G., & van Meijgaard, E. (2008). Increase in hourly precipitation extremes beyond expectations from temperature changes. *Nature Geoscience*, *1*(8), 511–514. https://doi.org/10.1038/ngeo262

Lenderink, G., & van Meijgaard, E. (2010). Linking increases in hourly precipitation extremes to atmospheric temperature and moisture changes. *Environmental Research Letters*, *5*(2), 025208. https://doi.org/10.1088/1748-9326/5/2/025208

Maimone, M., Malter, S., Rockwell, J., & Raj, V. (2019). Transforming global climate model precipitation output for use in urban stormwater applications. *Journal of Water Resources Planning and Management*, *145*(6), 04019021. https://doi.org/10.1061/(ASCE)WR.1943-5452.0001071

Mamalakis, A., Langousis, A., Deidda, R., & Marrocu, M. (2017). A parametric approach for simultaneous bias correction and high-resolution downscaling of climate model rainfall, Water Resources Research. *Water Resources Research*, *53*(3), 2149–2170. https://doi.org/10.1002/2016wr019578

Meehl, G. A., Arblaster, J. M., & Tebaldi, C. (2005). Understanding future patterns of increased precipitation intensity in climate model simulations. *Geophysical Research Letters*, *32*(18). https://doi.org/10.1029/2005GL023680

Meehl, G. A., Washington, W. M., Arblaster, J. M., Hu, A., Teng, H., Tebaldi, C., et al. (2012). Climate system response to external forcings and climate change projections in CCSM4. *Journal of Climate*, *25*(11), 3661–3683. https://doi.org/10.1175/jcli-d-11-00240.1

Nakicenovic, N., Alcamo, J., Grubler, A., Riahi, K., Roehrl, R., Rogner, H.-H., & Victor, N. (2000). *Special report on emissions scenarios (SRES), a special report of Working Group III of the intergovernmental panel on climate change*. Cambridge University Press. Retrieved from https://www.ipcc.ch/site/assets/uploads/2018/03/sres-en.pdf

Nie, L., Lindholm, O., Lindholm, G., & Syversen, E. (2009). Impacts of climate change on urban drainage systems—A case study in Fredrikstad, Norway. *Urban Water Journal*, *6*(4), 323–332. https://doi.org/10.1080/15730620802600924

Panthou, G., Mailhot, A., Laurence, E., & Talbot, G. (2014). Relationship between surface temperature and extreme rainfalls: A multi-time-scale and event-based analysis. *Journal of Hydrometeorology*, *15*(5), 1999–2011. https://doi.org/10.1175/jhm-d-14-0020.1

Pfister, L., Kwadijk, J., Musy, A., Bronstert, A., & Hoffmann, L. (2004). Climate change, land use change and runoff prediction in the Rhine-Meuse basins. *River Research and Applications*, *20*(3), 229–241. https://doi.org/10.1002/rra.775

Rajagopalan, B., & Lall, U. (1999). A k-nearest-neighbor simulator for daily precipitation and other weather variables. *Water Resources Research*, *35*(10), 3089–3101. https://doi.org/10.1029/1999wr900028

Rajagopalan, B., Lall, U., & Tarboton, D. G. (1996). Nonhomogeneous Markov model for daily precipitation. *Journal of Hydrologic Engineering*, *1*(1), 33–40. https://doi.org/10.1061/(ASCE)1084-0699(1996)1:1(33)

Rodriguez-Iturbe, I., Cox, D. R., & Isham, V. (1987). Some models for rainfall based on stochastic point processes. *Proceedings of the Royal Society of London—Series A: Mathematical and Physical Sciences*, *410*(1839), 269–288. https://doi.org/10.1098/rspa.1987.0039

Rodriguez-Iturbe, I., Cox, D. R., & Isham, V. (1988). A point process model for rainfall: Further developments. *Proceedings of the Royal Society of London—Series A: Mathematical and Physical Sciences*, *417*(1853), 283–298. https://doi.org/10.1098/rspa.1988.0061

Schreider, S. Y., Smith, D. I., & Jakeman, A. J. (2000). Climate change impacts on urban flooding. *Climatic Change*, *47*(1), 91–115. https://doi.org/10.1023/a:1005621523177

Semadeni-Davies, A., Hernebring, C., Svensson, G., & Gustafsson, L. G. (2008). The impacts of climate change and urbanisation on drainage in Helsingborg, Sweden: Combined sewer system. *Journal of Hydrology*, *350*(1–2), 100–113. https://doi.org/10.1016/j.jhydrol.2007.05.028

Shamir, E., Megdal, S. B., Carrillo, C., Castro, C. L., Chang, H. I., Chief, K., et al. (2015). Climate change and water resources management in the upper Santa Cruz river, Arizona. *Journal of Hydrology*, *521*, 18–33. https://doi.org/10.1016/j.jhydrol.2014.11.062

Sharma, A., & Lall, U. (1999). A nonparametric approach for daily rainfall simulation. *Mathematics and Computers in Simulation*, *48*(4–6), 361–371. https://doi.org/10.1016/S0378-4754(99)00016-6

Shaw, S. B., Royem, A. A., & Riha, S. J. (2011). The relationship between extreme hourly precipitation and surface temperature in different hydroclimatic regions of the United States. *Journal of Hydrometeorology*, *12*(2), 319–325. https://doi.org/10.1175/2011jhm1364.1

Solomon, S., Qin, D., Manning, M., Chen, Z., Marquis, M., Averyt, K. B., et al. (Eds.) (2007). Summary for policymakers, *Climate change 2007: The physical science basis*. IPCC.

Stern, R. D., & Coe, R. (1984). A model fitting analysis of daily rainfall data. *Journal of the Royal Statistical Society: Series A*, *147*(1), 1–34. https://doi.org/10.2307/2981736

Sun, Y., Solomon, S., Dai, A., & Portmann, R. W. (2007). How often will it rain? *Journal of Climate*, *20*(19), 4801–4818. https://doi.org/10.1175/jcli4263.1

Tebaldi, C., Hayhoe, K., Arblaster, J. M., & Meehl, G. A. (2006). Going to the extremes. *Climatic Change*, *79*(3–4), 185–211. https://doi.org/10.1007/s10584-006-9051-4

Teutschbein, C., & Seibert, J. (2013). Is bias correction of regional climate model (RCM) simulations possible for non-stationary conditions? *Hydrology and Earth System Sciences*, *17*(12), 5061–5077. https://doi.org/10.5194/hess-17-5061-2013

Trenberth, K. E. (2011). Changes in precipitation with climate change. *Climate Research*, *47*(1–2), 123–138. https://doi.org/10.3354/cr00953

Trenberth, K. E., & Shea, D. J. (2005). Relationships between precipitation and surface temperature. *Geophysical Research Letters*, *32*(14). https://doi.org/10.1029/2005GL022760

US EPA (Environmental Protection Agency). (2010). Climate change indicators in the United States.

VijayaVenkataRaman, S., Iniyan, S., & Goic, R. (2012). A review of climate change, mitigation and adaptation. *Renewable and Sustainable Energy Reviews*, *16*(1), 878–897. https://doi.org/10.1016/j.rser.2011.09.009

Visser, J. B., Wasko, C., Sharma, A., & Nathan, R. (2020). Resolving inconsistencies in extreme precipitation-temperature sensitivities. *Geophysical Research Letters*, *47*(18), e2020GL089723. https://doi.org/10.1029/2020GL089723

Wasko, C., Pui, A., Sharma, A., Mehrotra, R., & Jeremiah, E. (2015). Representing low-frequency variability in continuous rainfall simulations: A hierarchical random Bartlett Lewis continuous rainfall generation model. *Water Resources Research*, *51*(12), 9995–10007. https://doi.org/10.1002/2015WR017469

Wasko, C., & Sharma, A. (2015). Steeper temporal distribution of rain intensity at higher temperatures within Australian storms. *Nature Geoscience*, *8*(7), 527–529. https://doi.org/10.1038/ngeo2456

Wasko, C., & Sharma, A. (2017). Continuous rainfall generation for a warmer climate using observed temperature sensitivities. *Journal of Hydrology*, *544*, 575–590. https://doi.org/10.1016/j.jhydrol.2016.12.002

Wasko, C., Sharma, A., & Johnson, F. (2015). Does storm duration modulate the extreme precipitation-temperature scaling relationship? *Geophysical Research Letters*, *42*(20), 8783–8790. https://doi.org/10.1002/2015GL066274

Westra, S., Alexander, L. V., & Zwiers, F. W. (2013). Global increasing trends in annual maximum daily precipitation. *Journal of Climate*, *26*(11), 3904–3918. https://doi.org/10.1175/jcli-d-12-00502.1

Westra, S., Evans, J. P., Mehrotra, R., & Sharma, A. (2013). A conditional disaggregation algorithm for generating fine time-scale rainfall data in a warmer climate. *Journal of Hydrology*, *479*, 86–99. https://doi.org/10.1016/j.jhydrol.2012.11.033

Wilks, D. S. (1998). Multisite generalization of a daily stochastic precipitation generation model. *Journal of Hydrology*, *210*(1), 178–191. https://doi.org/10.1016/S0022-1694(98)00186-3

Wilks, D. S. (2010). Use of stochastic weather generators for precipitation downscaling. *Wiley Interdisciplinary Reviews-Climate Change*, *1*(6), 898–907. https://doi.org/10.1002/wcc.85

Wilks, D. S., & Wilby, R. L. (1999). The weather generation game: A review of stochastic weather models. *Progress in Physical Geography*, *23*(3), 329–357. https://doi.org/10.1191/030913399666525256

Yu, Z., Miller, S., Montalto, F., & Lall, U. (2018). The bridge between precipitation and temperature–pressure change events: Modeling future non-stationary precipitation. *Journal of Hydrology*, *562*, 346–357. https://doi.org/10.1016/j.jhydrol.2018.05.014

Zhang, C., Wu, S., Li, T., Yu, Z., & Bian, J. (2022). Interpreting the trends of extreme precipitation in Florida through pressure change. *Remote Sensing*, *14*(6), 1410. https://doi.org/10.3390/rs14061410